Suppression of thermal conductivity in graphene nanoribbons with rough edges

Alexander V. Savin,[1,2] Yuri S. Kivshar,[2] and Bambi Hu[3,4]
[1]*Semenov Institute of Chemical Physics, Russian Academy of Sciences, Moscow 119991, Russia*
[2]*Nonlinear Physics Center, Research School of Physics and Engineering, Australian National University, Canberra, Australian Capital Territory 0200, Australia*
[3]*Department of Physics, University of Houston, Houston, Texas 77204-5005, USA*
[4]*Centre for Nonlinear Studies, The Beijing-Hong Kong-Singapore Joint Centre for Nonlinear and Complex Systems (Hong Kong), Hong Kong Baptist University, Kowloon Tong, Hong Kong, China*
(Received 25 June 2010; revised manuscript received 27 September 2010; published 10 November 2010)

We analyze numerically thermal conductivity of graphene nanoribbons with perfect and rough edges. We demonstrate that edge roughness can suppress thermal conductivity by two orders of magnitude. This effect is associated with the edge-induced energy localization and suppression of the phonon transport, and it becomes more pronounced for longer nanoribbons and low temperatures.

DOI: 10.1103/PhysRevB.82.195422 PACS number(s): 65.80.−g, 63.22.Gh

I. INTRODUCTION

The study of remarkable properties of graphite structures is one of the hot topics of nanoscience.[1] Graphene nanoribbons (GNRs) are effectively low-dimensional structures similar to carbon nanotubes but their main feature is the presence of edges. Due to the edges, GNRs can demonstrate many novel properties driven by their geometry and dependent on their width and helicity. A majority of the current studies of GNRs is devoted to the analysis of electronic and magnetic properties modified by the presence of edges, including the existence of the localized edge modes,[2,3] which are an analog of surface states in the two-dimensional geometry. The edges can support localized vibrational states in both linear and nonlinear regimes.[4,5]

The effect of surface disorder, e.g., stipulated by the edge roughness, on the electronic transport of GNRs has been discussed in several papers (see, e.g., Refs. 6–9). It was found that a relatively modest edge disorder is already sufficient to induce the conduction energy gap in the otherwise metallic nanoribbons and to lift any difference in the conductance between nanoribbons of different edge geometry, suggesting that this type of disorder can be very important for changing other fundamental characteristics of GNRs.

In addition to electronic properties, the thermal properties of graphene are also of both fundamental and practical importance. Several experiments[10,11] demonstrated that graphene has a superior thermal conductivity, likely underlying the high thermal conductivity known in carbon nanotubes.[12]

From the other hand, recent experiments demonstrated that thermal conductivity of silicon nanowires can be dramatically reduced by surface roughness.[13,14] For a qualitative explanation of this effect a simple phenomenological model was suggested in Ref. 15; this model describes a nanowire as a system of a finite number of interacting one-dimensional chains with the longitudinal oscillations, where roughness is modeled by randomly missed atoms in the edge chains. It was shown that superdiffusion of thermal energy in nanowires with atomically smooth edges is replaced by normal diffusion or subdiffusion in the case of rough edges, thus leading to a dramatic suppression of thermal conductivity. However, this simplest one-dimensional model is not applicable to the specific GRN geometry, and it does not allow to obtain any qualitative result for the effect of roughness on the thermal conductivity of nanoribbons.

Modeling of a thermal flow in ideal nanoribbons[16] suggests that the coefficient of thermal conductivity grows monotonically with the length. Similar to carbon nanotubes, the length dependence of thermal conductivity reveals the variation in a balance between ballistic and diffusive regimes of the heat conduction.

We notice that the heat transport in GRNs of different shapes was modeled in Ref. 17. In addition to rectangular structures, the authors considered triangular nanoribbons, the nanoribbons with defects (vacancies), as well as the case of rough edges when isolated vacancies are placed at the edges. However, the effect of rough edges on thermal conductivities of GNRs was not analyzed. Moreover, numerical studies based on the Nosé-Hoover thermostat do not always provide accurate results for the heat transfer.[18,19] For example, an alternative approach based on the Langevin thermostat does not confirm the predictions of Ref. 17 for significant thermal rectification in asymmetric nanoribbons and thermal conductivity of ~2000 W/mK for short (1.5 nm×5.7 nm) symmetric GRNs obtained by employing the Nosé-Hoover thermostat.

Recent studies of the thermal conductivity of GNRs with smooth and rough edges[20] employed an indirect method of the equilibrium molecular dynamics. In this case, the coefficient of thermal conductivity is defined through the Green-Kubo formula. It was shown that in the case of rough edges, the thermal conductivity coefficient is strong function of the ribbon width, and this shows the importance of the phonon scattering from the edges. However, the obtained estimate for the thermal conductivity κ=8000–20 000 W/mK contradicts to the results of the direct numerical modeling.[16]

Theoretical studies of the phonon thermal conductivity of single-layer graphene flakes were presented in Refs. 21 and 22. The calculations based on the Klemens approximation revealed that umklapp-limited thermal conductivity of graphene grows with increasing linear dimensions of graphene flakes. The phonon scattering on defects and

graphene edges has also been included into the model. It was found that thermal conductivity of single-layer graphene at room temperature is in the range of $\sim 2000-5000$ W/mK depending on the flake width, the defect concentration, and edge roughness.

Anderson localization in disordered nanoribbons was studied in Refs. 6–9 where it was shown that the transport characteristics, such as elastic mean-free path and localization length change rapidly with a growth of defect concentration at the edges. Therefore, we expect that the Anderson localization observed for quasi-one-dimensional disordered systems could suppress substantially thermal conductivity.

In this paper, we study thermal conductivity of isolated graphene nanoribbons with perfect and rough edges. The paper is organized as follows. In Sec. II we introduce our model and describe in detail our choice of interacting potentials for modeling of graphene structures, and introduce the effective density $d(0 \le d \le 1)$ characterizing the rough edges of the nanoribbon. In Sec. III we discuss the method of direct numerical modeling of heat transport along the nanoribbon, whereas in Sec. IV we discuss localization of oscillatory modes in the nanoribbons with rough edges and demonstrate that only the modes with the wavelength on the order of the nanoribbon's width are not localized. Section V is devoted to the study of thermal conductivity of nanoribbons with rough edges, where we show that the ballistic regime of the phonon transport in ideal nanoribbons is replaced by the energy superdiffusion in the presence of rough edges. In Sec. VI we analyze the dependence of the coefficient of thermal conductivity of a finite-length nanoribbon on the edge roughness, and demonstrate that the largest suppression of thermal conductivity occurs for the density $d=0.5$. Dependence of the thermal conductivity coefficient κ on the nanoribbon's length N is studied in Sec. VII, where we show that $\kappa(N)$ grows as a power-law function of the length, and the roughness changes the exponent of the power-law dependence. Section VIII discusses the dependence of thermal conductivity on temperature. Finally, Conclusion provides a summary of the results.

II. MODEL

We model a graphene nanoribbon as a planar strip of graphite, with the properties depending on the stripe width and chirality. We consider a hydrogen-terminated nanoribbon, where edge carbon atoms correspond to the molecular group CH—see Fig. 1. We consider such a group as a single effective particle (united atom) at the location of the carbon atom. Therefore, in our model of graphene nanoribbon we take the mass of atoms inside the strip as $M_0=12m_p$, and for the edge atoms we consider a large mass $M_1=13m_p$ (where $m_p=1.6603\times 10^{-27}$ kg is the proton mass).

The structure of the zigzag nanoribbon can be presented as a longitudinal repetition of the elementary cell composed K atoms (the even number $K \ge 4$). We use atom numbering shown in Fig. 2(a). In this case, each carbon atoms has a two-component index $\alpha=(n,k)$, where $n=0,\pm 1,\pm 2,\ldots$ stands for the number of the elementary cells, and $k=1,2,\ldots,K$ stands for the number atoms in the cell.

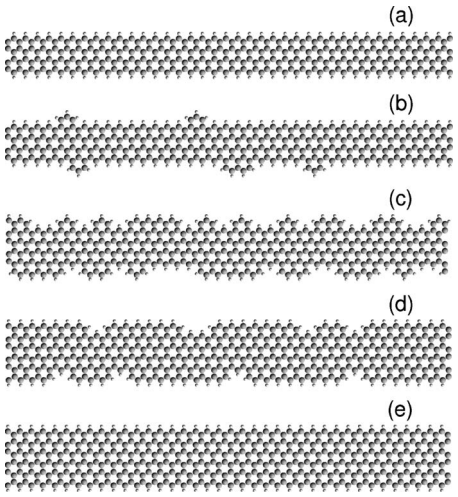

FIG. 1. Examples of hydrogen-terminated zigzag nanoribbons with rough edges for the density of the edge layers: (a) $d=0$, (b) $d=0.1$, (c) $d=0.5$, (d) $d=0.9$, and (e) $d=1$. Number of atoms in the elementary cell is $K=12$.

To model two rough edges we randomly delete some atoms with the second index $k=1$, 2 and $k=K-1$, K, see Figs. 1 and 2(a). When we remove an atom from the edge layer, the corresponding new edge atom should have two valent bonds with other carbon atoms, and one valent bond, with the hydrogen atom, see Figs. 1(b)–1(d). In this case all valent bonds in the nanoribbon will have the same length $\rho_0 \approx 1.4$ Å, and they can be described in a similar way by employing the same type of interaction potentials.

We notice that, if we consider nanoribbons without full hydrogen termination, then some edge valent bonds CC will be shorter and stronger ($\rho_0 \approx 1.2$ Å), see, e.g., Ref. 23. For describing these bonds we should employ other types of the interaction potentials, making the corresponding model rather complex. That is why, we use hydrogen-terminated nanoribbons are the most suitable for numerical modeling of the linear and nonlinear dynamics.

We characterize the degree of roughness by the density of its edge layers created by the atoms with the indices

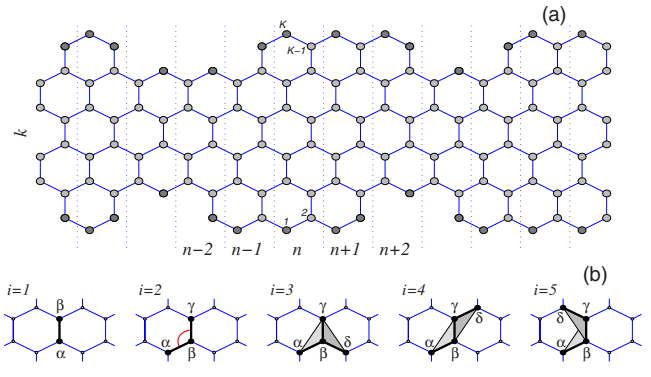

FIG. 2. (Color online) Schematic view (a) of a zigzag nanoribbon with rough edges and atom numbering. The edge unit atoms (CH groups) are shown as filled circles. Dotted lines separate the elementary cells of the nanoribbon. K is the number of atoms in the elementary cell. (b) Configurations of an ideal structure containing up to ith nearest-neighbor interactions for $i=1,\ldots,5$.

$\{(n,k)\}_{n=1}^{N}$, $k=1,2,K-1,K$. We define this value as $d=N_e/4N$, where N is the dimensionless length of the nanoribbon (the number of longitudinal cells) and N_e is the number of atoms in the edge layers (the atoms with the indices $k=1$, 2, $K-1$, and K). Several types of the nanoribbon structure are shown in Fig. 1 for different values of the density of rough edges. For $d=0$ [see Fig. 1(a)], the nanoribbon has a perfect structure with $K-4$ atoms in the elementary cell. When the value of the parameter d grows, the number of defects atoms in the edge layers grows as well, see Figs. 1(b)–1(d). For $d=1$ the nanoribbon again has a perfect structure but its width is increased, and it has K atoms in the elementary cell [Fig. 1(e)].

To describe the dynamics of nanoribbons with both ideal and rough edges, we present the system Hamiltonian in the form

$$H=\sum_{n=-\infty}^{+\infty}\sum_{k=1}^{K_n}\left[\frac{1}{2}M_{(n,k)}(\dot{\mathbf{u}}_{(n,k)},\dot{\mathbf{u}}_{(n,k)})+P_{(n,k)}\right], \tag{1}$$

where $K-4\leq K_n\leq K$ is the number of atoms in the nth elementary cell, M_α is the mass of the carbon atom with the index $\alpha=(n,k)$, $\mathbf{u}_\alpha=[x_\alpha(t),y_\alpha(t),z_\alpha(t)]$ is the radius vector of the carbon atom with the index α at the moment t. The term P_α describes the interaction of the atom with the index $\alpha=(n,k)$ with its neighboring atoms.

We mimic hydrogen H termination of the edges using a united atom approach, and describe the edge atomic groups CH as united atoms with mass $M_1=13m_p$ (for internal atoms we take $M_\alpha=M_0=12m_p$). This approach does not allow to describe high-frequency motion of the H atom (with the frequency $\omega_{\mathrm{CH}}\sim 3000\ \mathrm{cm}^{-1}$). However, this high-frequency motion should not affect much the thermal conductivity since the later is dominated by the phonons with much lower frequencies. We notice that high-frequency oscillations of the CH bonds can be described the methods of molecular dynamics only for very high temperatures, $T>\hbar\omega_{\mathrm{CH}}/k_B=4316$ K.

The potential $P_{(n,k)}$ depends on variations in bond length, bond angles, and dihedral angles between the planes formed by three neighboring carbon atoms, and it can be written in the form

$$P=\sum_{\Omega_1}U_1+\sum_{\Omega_2}U_2+\sum_{\Omega_3}U_3+\sum_{\Omega_4}U_4+\sum_{\Omega_5}U_5, \tag{2}$$

where Ω_i, with $i=1$, 2, 3, 4, 5 stand for the sets of configurations including up to nearest-neighbor interactions. Owing to a large redundancy, the sets only need to contain configurations of the atoms shown in Fig. 2(b), including their rotated and mirrored versions.

The potential $U_1(\mathbf{u}_\alpha,\mathbf{u}_\beta)$ describes the deformation energy due to a direct interaction between pairs of atoms with the indices α and β, as shown in Fig. 2(b). The potential $U_2(\mathbf{u}_\alpha,\mathbf{u}_\beta,\mathbf{u}_\gamma)$ describes the deformation energy of the angle between the valent bonds $\mathbf{u}_\alpha\mathbf{u}_\beta$ and $\mathbf{u}_\beta\mathbf{u}_\gamma$. Potentials $U_i(\mathbf{u}_\alpha,\mathbf{u}_\beta,\mathbf{u}_\gamma,\mathbf{u}_\delta)$, $i=3$, 4, 5, describes the deformation energy associated with a change in the effective angle between the planes $\mathbf{u}_\alpha,\mathbf{u}_\beta,\mathbf{u}_\gamma$ and $\mathbf{u}_\beta,\mathbf{u}_\gamma,\mathbf{u}_\delta$.

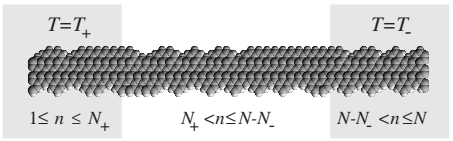

FIG. 3. Example of a hydrogen-terminated zigzag nanoribbon with rough edges with N longitudinal segments. First left N_+ segments are attached to the $T=T_+$ thermostat and the last right N_- segments are attached to the $T=T_-$ thermostat. Number of atoms in the elementary cell $K=12$ and density of the edge layers $d=0.5$.

We use the potentials employed in the modeling of the dynamics of large polymer macromolecules[24,25] for the valent bond coupling,

$$U_1(\mathbf{u}_1,\mathbf{u}_2)=\epsilon_1\{\exp[-\alpha_0(\rho-\rho_0)]-1\}^2,\quad \rho=|\mathbf{u}_2-\mathbf{u}_1|, \tag{3}$$

where $\epsilon_1=4.9632$ eV is the energy of the valent bond and $\rho_0=1.418$ Å is the equilibrium length of the bond; the potential of the valent angle

$$U_2(\mathbf{u}_1,\mathbf{u}_2,\mathbf{u}_3)=\epsilon_2(\cos\varphi-\cos\varphi_0)^2,$$

$$\cos\varphi=(\mathbf{u}_3-\mathbf{u}_2,\mathbf{u}_1-\mathbf{u}_2)/(|\mathbf{u}_3-\mathbf{u}_2|\cdot|\mathbf{u}_2-\mathbf{u}_1|) \tag{4}$$

so that the equilibrium value of the angle is defined as $\cos\varphi_0=\cos(2\pi/3)=-1/2$; the potential of the torsion angle

$$U_i(\mathbf{u}_1,\mathbf{u}_2,\mathbf{u}_3,\mathbf{u}_4)=\epsilon_i(1-z_i\cos\phi),$$

$$\cos\phi=(\mathbf{v}_1,\mathbf{v}_2)/(|\mathbf{v}_1|\cdot|\mathbf{v}_2|),$$

$$\mathbf{v}_1=(\mathbf{u}_2-\mathbf{u}_1)\times(\mathbf{u}_3-\mathbf{u}_2),$$

$$\mathbf{v}_2=(\mathbf{u}_3-\mathbf{u}_2)\times(\mathbf{u}_3-\mathbf{u}_4), \tag{5}$$

where the sign $z_i=1$ for the indices $i=3$, 4 (equilibrium value of the torsional angle $\phi_0=0$) and $z_i=-1$ for the index $i=5(\phi_0=\pi)$.

The specific values of the parameters are $\alpha_0=1.7889$ Å^{-1}, $\epsilon_2=1.3143$ eV, and $\epsilon_3=0.499$ eV, and they are found from the frequency spectrum of small-amplitude oscillations of a sheet of graphite.[26] According to the results of Ref. 27 the energy ϵ_4 is close to the energy ϵ_3, whereas $\epsilon_5\ll\epsilon_4(|\epsilon_5/\epsilon_4|<1/20)$. Therefore, in what follows we use the values $\epsilon_4=\epsilon_3=0.499$ eV and assume $\epsilon_5=0$, the latter means that we omit the last term in the sum [Eq. (2)].

III. METHODS

In order to model the heat transport, we consider the nanoribbon of a finite length with two ends places in thermostats kept at different temperatures, as shown schematically in Fig. 3. In order to calculate numerically the coefficient of thermal conductivity, we should calculate the heat flux at any cross section of the nanoribbon. Therefore, first we obtain the formula for calculating the longitudinal local heat flux.

We define the $3K_n$-dimensional coordinate vector $\mathbf{u}_n=\{x_{n,k},y_{n,k},z_{n,k}\}_{k=1}^{K_n}$ which determines the atom coordinates

of an elementary cell n, and then write Hamiltonian (1) in the form

$$H = \sum_n h_n = \sum_n \left[\frac{1}{2}(\mathbf{M}_n \dot{\mathbf{u}}_n, \dot{\mathbf{u}}_n) + P_n(\mathbf{u}_{n-1}, \mathbf{u}_n, \mathbf{u}_{n+1}) \right], \quad (6)$$

where the first term describes the kinetic energy of the atoms ($\mathbf{M}_n$ is diagonal mass matrix of the nth elementary cell), and the second term describes the interaction between the atoms in the cell and with the atoms of neighboring cells.

Hamiltonian (6) generates the system of equations of motion,

$$-\mathbf{M}_n \ddot{\mathbf{u}}_n = \mathbf{F}_n = \mathbf{P}_{1,n+1} + \mathbf{P}_{2,n} + \mathbf{P}_{3,n-1}, \quad (7)$$

where the function $\mathbf{P}_{i,n} = \mathbf{P}_i(\mathbf{u}_{n-1}, \mathbf{u}_n, \mathbf{u}_{n+1})$, $\mathbf{P}_i = \partial P(\mathbf{u}_1, \mathbf{u}_2, \mathbf{u}_3)/\partial \mathbf{u}_i$, $i=1, 2, 3$.

Local heat flux through the nth cross section, j_n, determines a local longitudinal energy density h_n by means of a discrete continuity equation, $\dot{h}_n = j_n - j_{n+1}$. Using the energy density from Eq. (6) and the motion equations [Eq. (7)], we obtain the general expression for the energy flux through the nth cross section of the nanotube, $j_n = (\mathbf{P}_{1,n}, \dot{\mathbf{u}}_{n-1}) - (\mathbf{P}_{3,n-1}, \dot{\mathbf{u}}_n)$.

For a direct modeling of the heat transfer along the nanoribbon, we consider a nanoribbon of a fixed length $(N-1)h$ with fixed ends. We place the first $N_+ = 40$ segments into the Langevin thermostat at $T_+ = 310$ K, and the last $N_- = 40$ segments, into the thermostat at $T_- = 290$ K—see Fig. 3. As a result, for modeling of the thermal conductivity we need integrating numerically the following system of equations:

$$\mathbf{M}_n \ddot{\mathbf{u}}_n = -\mathbf{F}_n - \Gamma \mathbf{M}_n \dot{\mathbf{u}}_n + \Xi_n^+, \quad \text{for } n = 2, \ldots, N_+,$$

$$\mathbf{M}_n \ddot{\mathbf{u}}_n = -\mathbf{F}_n, \quad \text{for } n = N_+ + 1, \ldots, N - N_-,$$

$$\mathbf{M}_n \ddot{\mathbf{u}}_n = -\mathbf{F}_n - \Gamma \mathbf{M}_n \dot{\mathbf{u}}_n + \Xi_n^-, \quad \text{for } n = N - N_- + 1, \ldots, N - 1, \quad (8)$$

where $\Gamma = 1/t_r$ is the damping coefficient (relaxation time $t_r = 0.1$ ps), and

$$\Xi_n^{\pm} = (\xi_{1,1}, \xi_{1,2}, \xi_{1,3}, \ldots, \xi_{K_n,1}, \xi_{K_n,2}, \xi_{K_n,3})$$

is $12K_n$-dimensional vector of normally distributed random forces normalized by conditions

$$\langle \xi_{n,i}^{\pm}(t_1) \xi_{l,j}^{\pm}(t_2) \rangle = 2M_{n,i} k_B T_{\pm} \delta_{nl} \delta_{ij} \delta(t_1 - t_2).$$

Details of this numerical procedure for modeling the thermal conductivity can be found in our earlier paper[28] devoted to the study of thermal conductivity of carbon nanotubes.

We select the initial conditions for system [Eq. (8)] corresponding to the ground state of the nanoribbon, and solve the equations of motion numerically tracing the transition to the regime with a stationary heat flux. At the inner part of the nanotube ($N_+ < n \le N - N_-$), we observe the formation of a temperature gradient corresponding to a constant flux. Distribution of the average values of temperature and heat flux along the nanotube can be found in the form

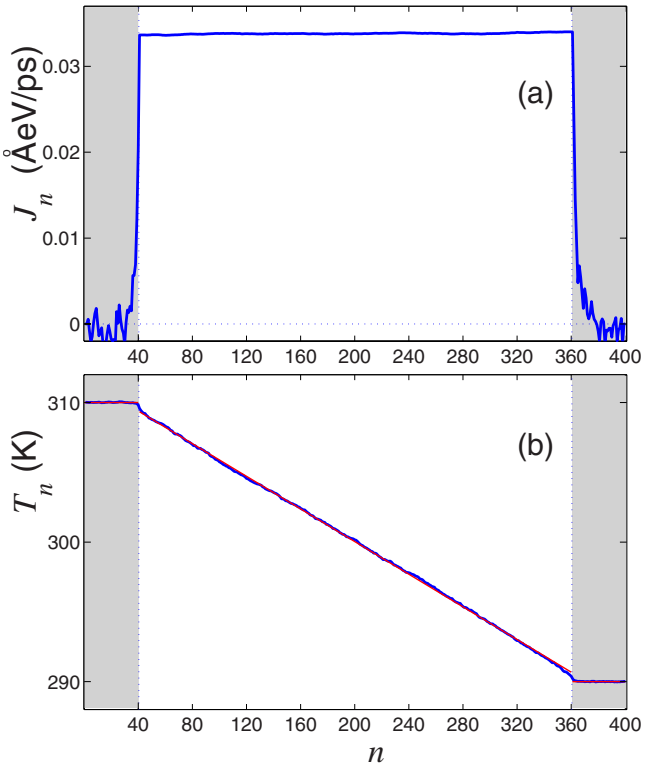

FIG. 4. (Color online) Distribution of (a) local heat flux J_n and (b) local average temperature T_n along a zigzag nanoribbon with rough edges ($K=12$ and density $d=0.5$). Length of the nanoribbon is $L=(N-1)h=98.1$ nm ($N=400$ and $h=0.246$ nm), and temperatures are $T_+=310$ K and $T_-=290$ K, the numbers of end segments interacting with the thermostats $N_{\pm}=40$ (corresponding fragments are shown in gray). Heat conductivity is $\kappa=16.2$ W/mK. For calculations we used 240 independent realizations of the nanoribbons with rough edges, and the dynamics was analyzed for the temporal interval of 4 ns.

$$T_n = \lim_{t\to\infty} \frac{1}{3K_n k_B t} \int_0^t [\mathbf{M}_n \dot{\mathbf{u}}_n(\tau), \dot{\mathbf{u}}_n(\tau)] d\tau,$$

$$J_n = \lim_{t\to\infty} \frac{h}{t} \int_0^t j_n(\tau) d\tau,$$

where k_B is the Boltzmann constant. For nanoribbons with rough edges we make the averaging not only in time but also on 240 independent realizations of the roughness.

Distribution of the temperature and local heat flux along the rough-edged nanoribbon is shown in Figs. 4(a) and 4(b). The heat flux in each cross section of the inner part of the nanoribbon should remain constant, namely, $J_n \equiv J$ for $N_+ < n \le N - N_-$. The requirement of independence of the heat flux J_n on a local position n is a good criterion for the accuracy of numerical simulations, as well as it may be used to determine the integration time for calculating the mean values of J_n and T_n. As follows from the figures, the heat flux remains constant along the central inner part of the nanoribbon.

A linear temperature gradient can be used to define the local coefficient of thermal conductivity,

$$\kappa(N_i) = (N - N_- - N_+ - 1)J/(T_{N_+ + 1} - T_{N - N_-})S,$$

where $N_i = N - N_- - N_+$ is the number of periods in the central part of the nanoribbon, $S = 2(D_y + 2r_C)r_C$ is the area of the nanoribbon cross section (nanoribbon width $D_y = [2 + 3d + 3(K-8)/4]\rho_0$, van der Waals carbon radius $r_C = 1.85$ Å). Using this definition, we can calculate the asymptotic value of the coefficient $\kappa = \lim_{N\to\infty} \kappa(N)$.

IV. MODE LOCALIZATION IN NANORIBBONS WITH ROUGH EDGES

For small displacements $\mathbf{v}(t) = \{\mathbf{v}_n(t)\}_{n=1}^N = \{\mathbf{u}_n(t) - \mathbf{u}_n^0\}_{n=1}^N$, where the vector $\mathbf{u}^0 = \{\mathbf{u}_n^0\}_{n=1}^N$ defines positions of atoms in the ground state of the ribbon, and the amplitude is small, $\|\mathbf{v}\| \ll \rho_0$, the motion equations [Eq. (7)] can be presented a system of linear equations $-\mathbf{B}\mathbf{v} = \mathbf{A}\mathbf{v}$, where $\mathbf{B}$ is the diagonal matrix of masses and $\mathbf{A}$ is a symmetric real matrix. To find the eigenmodes of the nanoribbon in the form $\mathbf{v} = A\mathbf{e}\exp(-i\omega t)$ we should solve an eigenvalue problem $(\mathbf{A} - \omega^2\mathbf{B})\mathbf{e} = 0$, where ω is the mode frequency, $A > 0$ is the mode amplitude, and the eigenmode vector $\mathbf{e} = \{\mathbf{e}_{n,k}\}_{n=1,k=1}^{N,K_n}$ is normalized by the condition $(\mathbf{e}, \mathbf{B}\mathbf{e}) = 1$.

To analyze eigenvalue oscillation, we define the distribution function of the oscillatory energy along nanoribbon as follows:

$$p_n = \sum_{k=1}^{K_n} M_{n,k}|\mathbf{e}_{n,k}|^2.$$

The energy distribution is normalized by the following condition, $\Sigma_{n=1}^N p_n = (\mathbf{e}, \mathbf{B}\mathbf{e}) = 1$. We introduce the parameter characterizing the energy localization in the nanoribbon as follows, $D = 1/\Sigma_{n=1}^N p_n^2$. This parameter characterizes the dimensionless width of the energy localization in the nanoribbon. If the vibrational mode is localized only on one elementary cell (i.e., there exists an cell n_0 for which $p_{n_0} = 1$), the width is $D = 1$. In the opposite limit, when the vibrational energy is distributed equally on all atoms ($p_n \equiv 1/N$), we have $D = N$ so that in a general case $1 \le D \le N$.

First, we study an ideal nanoribbon of a fixed length with $N = 300$ and $K = 10$. To find all oscillatory eigenmodes of such a structure, we solve the generalized eigenvalue problem with real symmetric matrices of the order $3NK \times 3NK$. The nanoribbon has $3NK = 9000$ eigenmodes with the eigenfrequencies $0 \le \omega \le 1600$ cm^{-1}. Dependence of the width of the eigenmode D vs its frequency ω is shown in Fig. 5(a). As follows from that figure, practically all eigenmodes of the nanoribbon has the width $200 \le D \le 300$ comparable with the length of the nanoribbon. There exist only a few modes localized at the edge atoms of the nanoribbon with the indices $n = 1$ and $n = N$; more detailed analysis of such localized surface modes can be found in Ref. 4. However, for the periodic boundary conditions no surface states occur, and all modes have the width $200 \le D \le 300$.

For the nanoribbon with rough edges ($N = 300, K = 12, d = 0.5$), most of eigenmodes is localized [see Fig. 5(a), curve 2], and only low-frequency oscillatory modes with the wavelength on the order of the nanoribbon length are not much affected by the edge roughness. While the frequency spectrum of the nanoribbons with both perfect and rough edges remains unchanged, its structure becomes "smoothen" in the case of disorder, see Figs. 5(b) and 5(c).

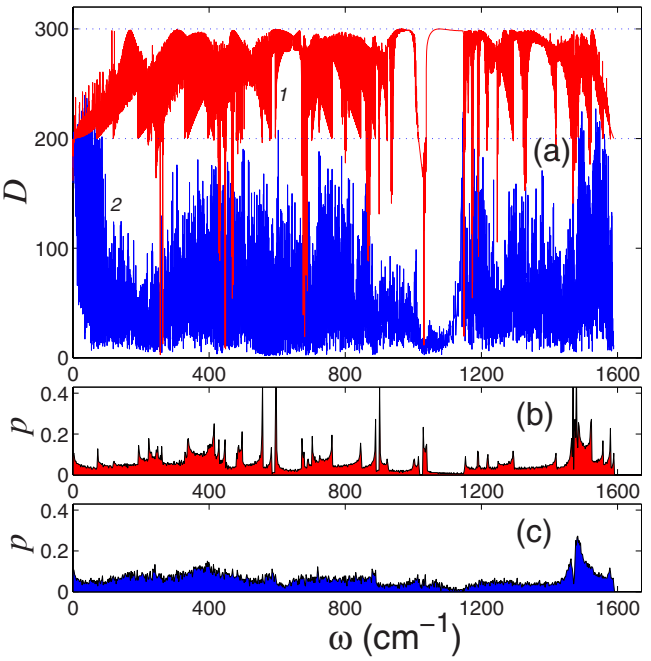

FIG. 5. (Color online) Dependence (a) of the width of eigenvalue oscillation D on the frequency ω for an ideal nanoribbon (curve 1, $N = 300$, $K = 10$, and $d = 1$) and nanoribbon with rough edges (curve 2, $N = 300$, $K = 12$, and $d = 0.5$). Spectral density $p(\omega)$ for (a) ideal and (b) disordered nanoribbon. For convenience, the density is normalized by the condition $\int_0^\infty p(\omega)d\omega = 100$.

This analysis of linear eigenmodes of the nanoribbon reveals that in the case of rough edges majority of vibrational modes are localized as functions of the longitudinal index n. This means that in our system we observe the manifestation of the Anderson localization due to the edge disorder, earlier discussed only for the wave transmission in surface-disordered waveguides.[29,30] Only the modes with the wavelength on the order of the nanoribbon length are not localized. As a result, we expect that the edge disorder should lead to suppression of phonon transport and dramatic reduction in the thermal conductivity.

V. ENERGY DIFFUSION IN NANORIBBONS WITH ROUGH EDGES

Now we analyze how the structure of the nanoribbon edges affects the phonon transport. We take the nanoribbon with $N = 2000$ cells (corresponding to the dimension length $L = Nh = 492$ nm), heat its central part with $N' = 20$ to the temperature $T = 30$ K, and study the heat transfer along the nanoribbon. Our numerical results show that random change in the edge structure (the edge roughness) leads to a substantial change in the heat transport, see Fig. 6, and the energy spreads much slower than in the case of ideal ribbon.

To characterize the energy diffusion we study the temporal dependence of the mean spatial width of the energy distribution along the nanoribbon, defined as

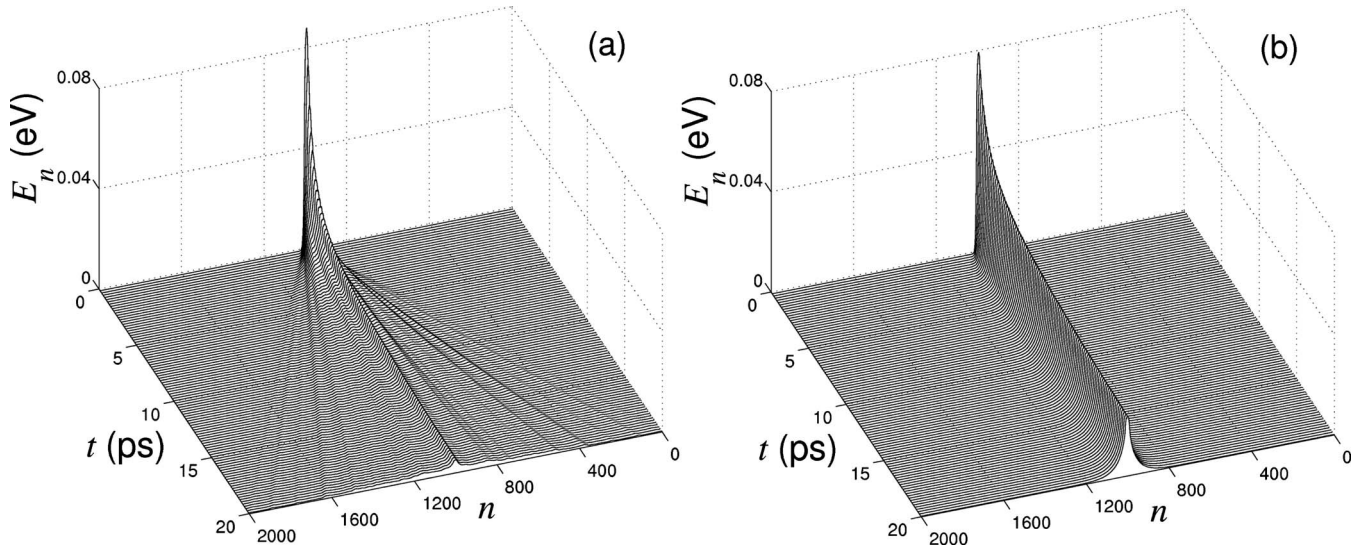

FIG. 6. Spreading of the heat pulse (initial width $L=20h$, amplitude $T_a=30$ K) in (a) nanoribbon (width $K=12$) with ideal edges (density $d=1$) and (b) in nanoribbon with rough edges ($K=12$ and $d=0.7$). The dependence of site energy E_n on time t is shown. Averaging was performed for 1000 independent realization of the rough edges.

$$\sigma^2(t) = \langle \Delta x^2 \rangle = \sum_{n=1}^{N} [n - (N+1)/2] p_n,$$

where a series $\{p_n = E_n/\bar{E}\}_{n=1}^{N}$, $\bar{E} = \Sigma_n E_n$, defines the energy distribution along the nanoribbon. To increase the accuracy for calculating the value σ^2 we carry out the averaging procedure over 10^3 independent realizations of the initially thermalized central part of the ribbon. The corresponding temporal dependence of σ^2 is shown in Fig. 7. Generally, the energy profile spreads as

$$\sigma^2(t) = 2Dt^{\alpha}, \quad \text{with degree } 0 < \alpha \leq 2.$$

Following this definition, we find for low temperatures that an ideal nanotube ($d=0,1$) generates the exponent $\alpha=2$, which corresponds to ballistic flow of thermal energy along the ribbon, and the thermal energy pulse propagates as a diverging packet of noninteracting phonons [see Figs. 6(a) and 7, curve 1]. In the nanotube with rough edge, this ballistic flow is replaced by superdiffusion of energy with the exponent α approaching 1. The lowest value $\alpha=1.08$ is achieved for the roughness density $d=0.7$, see Fig. 6(b) and 7, curve 2.

Our results suggest that the exponent $\alpha>1$ for any value of the edge roughness. This means that the roughness-induced edge disorder does not lead to the Anderson localization of all phonons in the ribbon since for the completely localized states we should obtain subdiffusion when $\alpha<1$.[15] Thus, the edge disorder leads to the suppression of the phonon transport and therefore it should affect dramatically the thermal conductivity of the graphene nanoribbons with rough edges.

VI. DEPENDENCE OF THERMAL CONDUCTIVITY ON THE EDGE ROUGHNESS

Our numerical results demonstrate that the thermal conductivity of graphene nanoribbon depends crucially on the degree of edge roughness. In spite of the fact that the nanoribbon has an ideal internal structure, its thermal conductivity is reduced dramatically, and it becomes much lower that the conductivity of an ideal nanoribbon of the same width.

Distribution of the thermal flow J_n and local temperature T_n along the nanoribbon with rough edges (for the density $d=0.5$ and width $K=12$) is presented in Figs. 4(a) and 4(b). In comparison with the ideal nanoribbon (not shown), the edge disorder leads to reduction in the thermal flow in at least ten times, as well as it changes the temperature profile along the nanoribbon. In addition, in an ideal nanoribbon we observe thermal resistance at the edges placed into a thermostat, which disappears in the case of rough surfaces. As a result, for the length $L=(N-N_--N_+)h$ $=78.7$ nm,($N=400$, $N_{\pm}=40$) the coefficient of thermal conductivity of the nanoribbon with rough edges is found as

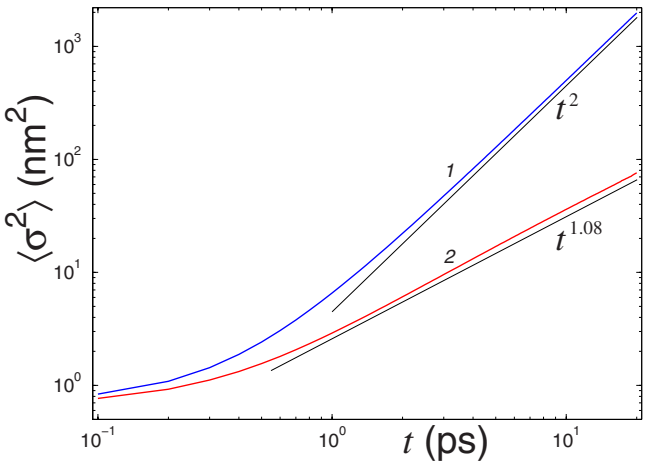

FIG. 7. (Color online) Root-mean-square spatial width of energy distribution σ^2 along nanoribbon versus time, t, for the nanoribbon with (a) ideal edges ($K=12$ and $d=1$) and (b) rough edges ($K=12$ and $d=0.7$).

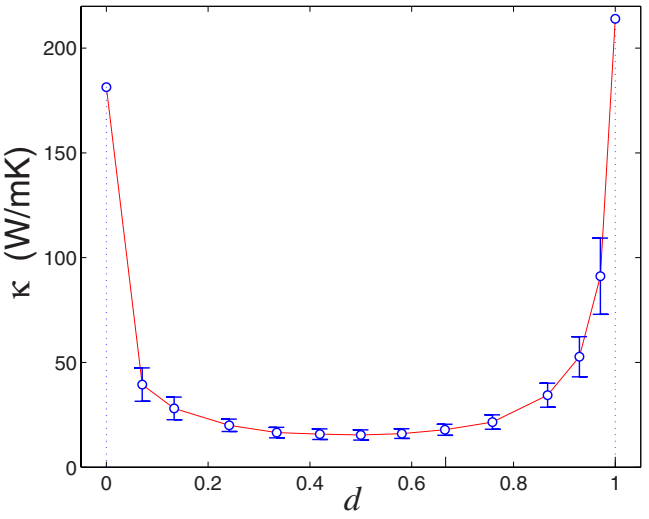

FIG. 8. (Color online) Dependence of the coefficient of thermal conductivity κ of a finite nanoribbon with rough edges ($K=12$, $N=240$, $N_{\pm}=20$, $T_{+}=310$ K, and $T_{-}=290$ K) on the density d. For calculation of κ we employed 120 independent realizations of the rough surfaces with the fixed density d. Thermal conductivity was calculated from the temporal evolution during 3 ns.

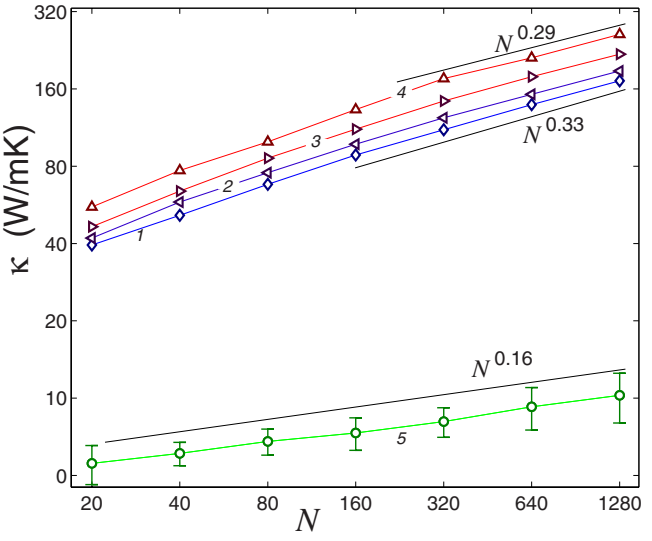

FIG. 9. (Color online) Dependence of the coefficient of thermal conductivity κ on the length of the central part of the nanoribbon N for ideal nanoribbon with $K=8$, 12, 20, 40 (curve 1, 2, 3, 4) and for rough edges nanoribbon with $K=12$ and $d=0.5$ (curve 5). For calculating the value of κ we employ 120 independent realizations of the rough edges and analyze the dynamics for 4 ns.

$\kappa=16.2$ W/mK that is in 15 times lower than the thermal conductivity of an ideal nanoribbon, $\kappa=247$ W/mK (density $d=1$ and width $K=12$).

Dependence of the coefficient of thermal conductivity κ on the degree of roughness characterized by the parameter d is shown in Fig. 8 for $K=12$, $N=240$, and $N_{\pm}=20$. As follows from this figure, the thermal conductivity will be the lowest for the densities $0.13<d<0.83$. The maximum is observed for $d=1$ and $d=0$ when we have ideal nanoribbons with $K=12$ and $K=8$ atoms in an elementary cell, respectively. The minimum is observed for the density $d=0.5$.

VII. DEPENDENCE OF THERMAL CONDUCTIVITY ON THE LENGTH

Below we study in more detail the thermal conductivity of rough-edged nanoribbons with the roughness density $d=0.5$. The corresponding structure of this nanoribbon is shown in Figs. 1(c) and 3.

Our numerical modeling described above demonstrates that for $T=300$ K the thermal conductivity of an ideal nanoribbon grows with its length L as a power-law function,

$$\kappa(N) \sim N^{\beta} \quad \text{for } N \to \infty, \tag{9}$$

where $\beta \approx 1/3$. The value of exponent β is almost independent on the nanoribbon width, and it changes slightly when the width increases, see Fig. 9. We notice that the general power-law dependence [Eq. (9)] is also valid for carbon nanotubes, however the value of the exponent β depends on the nanotube radius.[28] When the radius grows, the exponent β changes from the value $\beta=0.38$ for the nanotubes (5, 0), (3, 0) with the smallest radius $R=2$ Å to the value $\beta=0.14$ for nanotubes with the radius $R=8$ Å.

Our results for the coefficient of thermal conductivity of ideal nanoribbons $\kappa(N)$ agree well with the results of numerical modeling using the so-called Tersoff potential,[16] however they contradict to much higher values obtained in Ref. 17. We have checked those results by employing the Langevin thermostat, and we come to the conclusion that the main results of Ref. 17, namely, significant thermal rectification in asymmetric nanoribbons and large values of heat conductivity for short ideal nanoribbons, are results of incorrect use of the Nosé-Hoover thermostat.

We notice that the dependence [Eq. (9)] agree with the experimental estimate of thermal conductivity of graphene $\kappa \sim 3080-5150$ W/mK.[10] As follows from Fig. 9, the coefficient of thermal conductivity grows monotonically with the width of the nanoribbon so that the thermal conductivity of a planar sheet should be much higher than that of a nanoribbon. In accord with our results, for the nanoribbon with the width $D=4.1$ nm($K=40$) such values of thermal conductivity are achieved for the length $L \sim 50$ μm.

In contrast, the thermal conductivity of a nanoribbon with rough edges grows much slower, and for the parameters $K=12$, $d=0.5$ the power-law dependence [Eq. (9)] has the exponent $\beta=0.16$—see Fig. 9, curve 5. This difference grows with the length of the nanoribbon. For example, for $L=4.91$ nm($N=100$, $N_{\pm}=40$), a ratio between the coefficient of thermal conductivity of rough edge nanoribbon ($K=12$, $d=0.5$), κ_r, and ideal ($K=10$, $d=1$) nanoribbon of the same area, κ_i, is $\gamma=\kappa_r/\kappa_i=0.15$ but for the length $L=314.4$ nm this ratio becomes much smaller, $\beta=0.06$.

We notice that by adding new layers to the nanoribbon we change the thermal conductivity due to the cross-plane coupling of low-energy phonons and a change in the phonon umklapp scattering.[31] Therefore, we expect that multilayered nanoribbons will demonstrate even stronger suppression of thermal conductivity due to edge roughness.

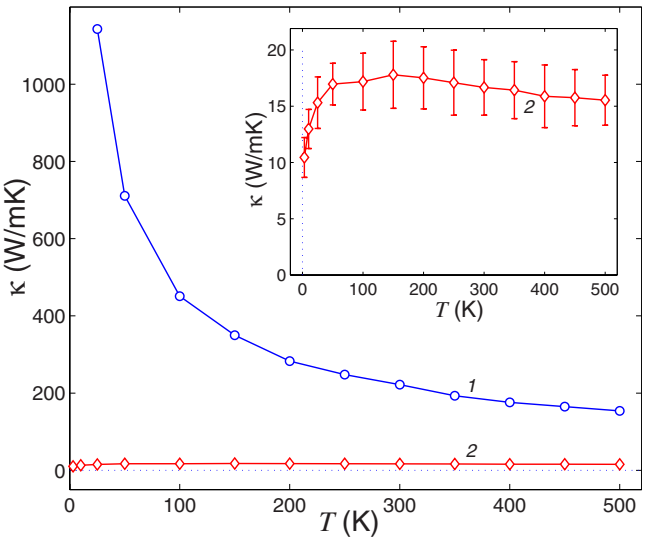

FIG. 10. (Color online) Dependence of the thermal conductivity coefficient κ on the temperature T for the ideal finite nanoribbon (curve 1, width $K=8$) and for edge-disordered nanoribbon (curve 2, width $K=10$ and $d=0.5$). Length of the central part $L=320h=78.6$ nm ($N=400$, $N_{\pm}=40$). For calculating κ (curve 2) we use 120 independent realizations of the rough edges and analyze the temporal evolution during 4 ns.

VIII. DEPENDENCE OF THERMAL CONDUCTIVITY ON TEMPERATURE

Now we study how this suppression of thermal conductivity depends on temperature. For an ideal nanoribbon, the coefficient of thermal conductivity grows monotonically when temperature decreases (see Fig. 10, curve 1) so that for $T\to 0$ we obtain $\kappa\to\infty$. This is related to the fact that the dynamics of nanoribbons approached the dynamics of one-dimensional linear system with infinite thermal conductivity. In contrast, for the nanoribbon with rough edges we observe that for $T>100$ K its thermal conductivity depends only weakly on temperature, see Fig. 10, curve 2. This result is explained by the fact that in the edge-disordered nanoribbon a majority of linear vibrational modes becomes localized due to the edge disorder, and the phonon transport is suppressed.

At low temperatures the system is described well by the linear approximation. In an ideal nanoribbon, the heat transfer occurs through a ballistic flow of phonons. As a result, the coefficient of thermal conductivity κ grows monotonically when temperature decreases, namely, $\kappa(T)\to\infty$ when $T\to 0$. In a finite-width nanoribbon with rough edges the heat energy is transferred at low temperature through harmonic oscillations mainly localized at the nanoribbon edges. Therefore, the ballistic flow of phonons in ideal nanoribbon is replaced by the energy subdiffusion in the nanoribbon with rough edges. This effect is enhanced for low temperatures. Indeed, when temperature decreases, nonlinear effects such as phonon-phonon scattering disappear, so that only ballistic flow of phonons remains in an ideal nanoribbon, so that thermal conductivity monotonically increases, whereas in the nanoribbon with rough edges phonons become scattered by inhomogeneous edges and the thermal conductivity saturates, see Fig. 10, curve 2.

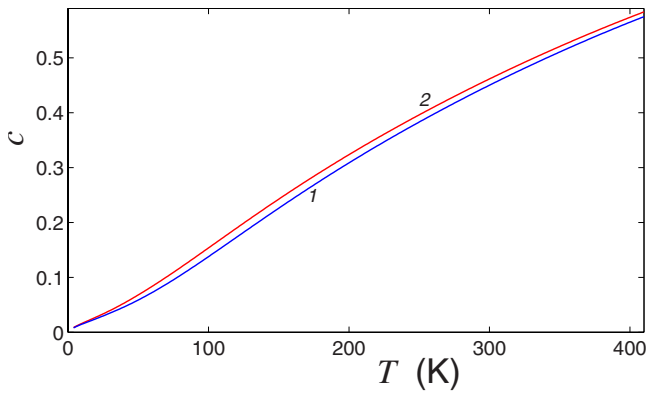

FIG. 11. (Color online) Temperature dependence of dimensionless specific heat c of ideal carbon nanoribbon (curve 1, $N=300$, $K=10$, and $d=1$) and nanoribbon with rough edges (curve 2, $N=300$, $K=12$, and $d=0.5$).

As a result, the ratio $\gamma=\kappa_r/\kappa_i$ decays monotonically. For example, for the nanoribbon with the length $L=78.6$ nm, at $T=500$ K this ratio is $\gamma=0.10$, at $T=300$ K, we have $\gamma=0.077$, at $T=100$ K we obtain $\gamma=0.036$, at $T=50$ K we find $\beta=0.021$, and at $T=25$ K, we have $\gamma=0.012$ (i.e., the thermal conductivity is reduced by two orders).

We should mention that the temperature dependence of the thermal conductivity found above is obtained in the framework of classical molecular-dynamics model, which does not take into account quantum effects of "frozen" high-frequency oscillations (and it requires substantial modifications[32]). In real crystals at low temperatures, thermal conductivity decays monotonically when $T\to 0$. This is explained by the fact that at low temperatures the temperature dependence of thermal conductivity is defined mainly by the temperature dependence of thermal capacity.

In classical mechanics, the thermal capacity of phonons does not depend on temperature, whereas in quantum mechanics such a dependence is defined by the formula $C(\omega,T)=k_B F_E(\omega,T)$, where the Einstein function

$$F_E(\omega,T)=\left(\frac{\hbar\omega}{k_B T}\right)^2\frac{\exp(\hbar\omega/k_B T)}{[\exp(\hbar\omega/k_B T)-1]^2},$$

where ω is the phonon frequency. For $T\to 0$, Einstein function $F_E\to 0$. The dimensionless thermal capacity is defined by the formula,

$$c(T)=\int_0^\infty F_E(\omega,T)p(\omega)d\omega,$$

where $p(\omega)$ is the density of the frequency spectrum normalized by the condition $\int_0^\infty p(\omega)d\omega=1$.

The frequency spectrum density of the nanoribbon with rough edges does not differ much from the density of an ideal nanoribbon of the same width, see Figs. 5(a) and 5(b). Therefore, the temperature dependencies for the dimensionless thermal capacity $c(T)$ do not differ much as well. In the nanoribbon with rough edges we observe only slightly increased capacity, see Fig. 11. As a result, we expect that quantum effect for low-temperature thermal conductivity

will be similar for nanoribbons with both perfect and rough edges. Thus, the ratio of conductivities κ_r/κ_i should remain valid even in the quantum regime. Indeed, in the quantum limit both thermal conductivities κ_r and κ_i vanishes for $T\rightarrow 0$ but its ratio will remain almost unchanged being close to the value obtained by means of a classical model.

IX. CONCLUSIONS

We have studied numerically thermal conductivity of graphene nanoribbons with perfect and rough edges. We have demonstrated that in nanoribbons with rough edges only the modes with the wavelengths comparable to the nanoribbon's width contribute to the heat transport, and a majority of oscillatory eigenmodes is localized and do not contribute to thermal conductivity. Thus, a disordered structure of the nanoribbon edges leads to a qualitative change in the heat transport, and the ballistic flow of phonons usually observed in ideal nanoribbons is suppressed substantiality in the case of rough edges being replaced by the energy superdiffusion.

Our results suggest that thermal conductivity of nanoribbons with perfect and rough edges is described by similar power-law dependencies on the ribbon's length. However, in the case of rough edges the coefficient of thermal conductivity κ_r is always smaller than the corresponding coefficient κ_i for an ideal nanoribbon of the same width. When the nanoribbon's length grows, κ_r increases slower than κ_i so that the ratio κ_r/κ_i decays monotonically with length and growths with temperature since the suppression of the phonon transport by rough edges is stronger for low temperatures. As a result, nanoribbons with ideal edges can play a role of highly efficient conductors while nanoribbons with rough edges can be employed as efficient thermal resistors.

ACKNOWLEDGMENTS

Alexander Savin acknowledges a hospitality of the Center for Nonlinear Studies of the Hong Kong Baptist University and Nonlinear Physics Center of the Australian National University where this work has been conducted. This work was supported by the Australian Research Council.

[1] M. I. Katsnelson, Mater. Today **10**, 20 (2007).
[2] G. Lee and K. Cho, Phys. Rev. B **79**, 165440 (2009).
[3] M. Engelund, J. A. Fürst, A. P. Jauho, and M. Brandbyge, Phys. Rev. Lett. **104**, 036807 (2010).
[4] A. V. Savin and Yu. S. Kivshar, Phys. Rev. B **81**, 165418 (2010).
[5] A. V. Savin and Yu. S. Kivshar, EPL **89**, 46001 (2010).
[6] M. Evaldsson, I. V. Zozoulenko, H. Xu, and T. Heinzel, Phys. Rev. B **78**, 161407(R) (2008).
[7] A. Cresti and S. Roche, Phys. Rev. B **79**, 233404 (2009).
[8] I. Martin and Ya. M. Blanter, Phys. Rev. B **79**, 235132 (2009).
[9] G. Schubert, J. Schleede, and H. Fehske, Phys. Rev. B **79**, 235116 (2009).
[10] S. Ghosh, I. Calizo, D. Teweldebrhan, E. P. Pokatilov, D. L. Nika, A. A. Balandin, W. Bao, F. Miao, and C. N. Lau, Appl. Phys. Lett. **92**, 151911 (2008).
[11] A. A. Balandin, S. Ghosh, W. Bao, I. Calizo, D. Teweldebrhan, F. Miao, and C. N. Lau, Nano Lett. **8**, 902 (2008).
[12] E. Pop, D. Mann, Q. Wang, K. Goodson, and H. Dai, Nano Lett. **6**, 96 (2006).
[13] A. L. Hochbaum, R. Chen, R. D. Delgado, W. Liang, E. C. Garnett, M. Najarian, A. Majumdar, and P. Yang, Nature (London) **451**, 163 (2008).
[14] A. I. Boukai, Y. Bunimovich, J. Tahir-Kheli, J.-K. Yu, W. A. Goddard III, and J. R. Heath, Nature (London) **451**, 168 (2008).
[15] Yu. A. Kosevich and A. V. Savin, EPL **88**, 14002 (2009).
[16] J. Shiomi and S. Maruyama, Int. J. Thermophys., online first (17 October 2008), DOI: 10.1007/s10765-008-0516-8.
[17] J. Hu, X. Ruan, and Y. P. Chen, Nano Lett. **9**, 2730 (2009).
[18] A. Fillipov, B. Hu, B. Li, and A. Zeltser, J. Phys. A **31**, 7719 (1998).
[19] J. Chen, G. Zhang, and B. Li, J. Phys. Soc. Jpn. **79**, 074604 (2010).
[20] W. J. Evans, L. Hu, and P. Keblinski, Appl. Phys. Lett. **96**, 203112 (2010).
[21] D. L. Nika, E. P. Pokatilov, A. S. Askerov, and A. A. Balandin, Phys. Rev. B **79**, 155413 (2009).
[22] D. L. Nika, S. Ghosh, E. P. Pokatilov, and A. A. Balandin, Appl. Phys. Lett. **94**, 203103 (2009).
[23] T. Kawai, Y. Miyamoto, O. Sugino, and Y. Koga, Phys. Rev. B **62**, R16349 (2000).
[24] D. W. Noid, B. G. Sumpter, and B. Wunderlich, Macromolecules **24**, 4148 (1991).
[25] A. V. Savin and L. I. Manevitch, Phys. Rev. B **67**, 144302 (2003).
[26] A. V. Savin and Yu. S. Kivshar, EPL **82**, 66002 (2008).
[27] D. Gunlycke, H. M. Lawler, and C. T. White, Phys. Rev. B **77**, 014303 (2008).
[28] A. V. Savin, B. Hu, and Yu. S. Kivshar, Phys. Rev. B **80**, 195423 (2009).
[29] V. D. Freylikher, N. M. Makarov, and I. V. Yurkevich, Phys. Rev. B **41**, 8033 (1990).
[30] J. A. Sánchez-Gil, V. Freilikher, I. Yurkevich, and A. A. Maradudin, Phys. Rev. Lett. **80**, 948 (1998).
[31] S. Ghosh, W. Bao, D. L. Nika, S. Subrina, E. P. Pokatilov, C. N. Lau, and A. A. Balandin, Nature Mater. **9**, 555 (2010).
[32] S. Buyukdagli, A. V. Savin, and B. Hu, Phys. Rev. E **78**, 066702 (2008).